Research Square

Preprints are preliminary reports that have not undergone peer review.
They should not be considered conclusive, used to inform clinical practice,
or referenced by the media as validated information.

Heteroepitaxial Single-Crystal Diamond on Sapphire: A Review

Genzhuang Li
Yili Normal University
Xuejun Li
Yili Normal University
Tiannan Chen
Yili Normal University
Weiwei Hu
Xinjiang Spen Solar Energy Technology Co., Ltd.
Aochen Du
Yili Normal University
Lai Wei
Yili Normal University
Liuan Li
liliuan@jlu.edu.cn
Jilin University

Systematic Review

Keywords: diamond, heteroepitaxy, sapphire, iridium, single crystal, microwave plasma CVD, stress control, twinning

Posted Date: October 7th, 2026

DOI: https://doi.org/10.21203/rs.3.rs-11007002/v1

License: This work is licensed under a Creative Commons Attribution 4.0 International License.
Read Full License

Additional Declarations: No competing interests reported.

Heteroepitaxial Single-Crystal Diamond on Sapphire: A Review

Genzhuang Li[1,2], Xuejun Li[1], Tiannan Chen[1], Weiwei Hu[3], Aochen Du[1,2,*], Lai Wei[1,2,*], Liuan Li[4,*]

1 Xinjiang Laboratory of Phase Transitions and Microstructures in Condensed Matter Physics, College of Physical Science and Technology, Yili Normal University, Yining, Xinjiang, 835000, China

2 Yili Engineering Research Center of Green Silicon-based Materials, College of Physical Science and Technology, Yili Normal University, Yining, Xinjiang, 835000, China

3 Xinjiang Spen Solar Energy Technology Co., Ltd., Yining, Xinjiang, 835000, China

4 State Key Laboratory of High Pressure and Superhard Materials, College of Physics, Jilin University, Changchun 130012, China

* Correspondence: Aochen Du (24083@ylnu.edu.cn), Lai Wei (lweiphy@sina.com), Liuan Li (liliuan@jlu.edu.cn).

Abstract

Heteroepitaxial growth of single-crystal diamond on sapphire substrates is a key technical route toward large-size, high-quality diamond wafers. This paper systematically reviews the recent research progress in the preparation of Ir/sapphire composite substrates, heteroepitaxial growth of (001) and (111) oriented diamond, stress and defect control strategies, and device applications. Studies have shown that by optimizing the off-cut angle of sapphire substrates, annealing processes, and Ir deposition conditions, the crystal orientation of Ir films can be effectively regulated, thereby achieving the epitaxial growth of high-quality diamond. In particular, methods such as microneedle structures, Pd buffer layers, and SiO_2 nanosphere interlayers have significantly reduced the thermal mismatch stress and dislocation density, and free-standing single-crystal diamond films with a size of 2 inch or even larger have been successfully obtained. In terms of device applications, MOSFETs and Schottky barrier diodes based on heteroepitaxial diamond have demonstrated high breakdown voltage and high current density, proving their potential in the fields of power electronics and ultraviolet detection. Despite this progress, the control of twinning in (111)-oriented diamond, the alleviation of interfacial stress, and the uniformity over large dimensions remain central challenges for future research.

Keywords: diamond, heteroepitaxy, sapphire, iridium, single crystal, microwave plasma CVD, stress control, twinning

1. Introduction

Diamond is widely regarded as the ultimate semiconductor material due to its excellent physical properties, such as an ultra-wide bandgap (5.47 eV), high breakdown electric field (>10 MV/cm), extremely high thermal

conductivity (22 $W \cdot cm^{-1} \cdot K^{-1}$), and high carrier mobility (4500 $cm^2/V^{-1} \cdot s^{-1}$ for electrons and 3800 $cm^2/V^{-1} \cdot s^{-1}$ for holes). These superior properties make diamond an ideal candidate not only for next-generation high-power and high-frequency electronic devices but also for extreme-environment applications such as space exploration and deep-sea missions [1-3]. To fully utilize these excellent properties, it is crucial to obtain single-crystal diamond substrates with a size of 1 inch or more. Due to the limited size of commercial single-crystal diamond grown by the high-pressure high-temperature (HPHT) method, which is only 10 × 10 mm^2, microwave plasma chemical vapor deposition (MPCVD) is currently the most widely recognized method for preparing large-size, high-quality single-crystal diamond. After years of development, mosaic stitching and heteroepitaxy have become the main methods for achieving single-crystal diamond with a size of 2 inch or more. Stitching growth involves arranging multiple smaller substrates in a regular pattern to form a "large substrate", and then combining with MPCVD epitaxial growth to fuse them into a large-size single-crystal diamond. Currently, stitching growth has achieved single-crystal diamond of 2-3 inches with a dislocation density of approximately 10^4 cm^{-2}. However, numerous dislocations and accumulated stress remain in the stitching seam areas [4, 5]. The size of heteroepitaxial single-crystal diamond is limited only by the substrate size, making it easier to scale up than the stitching approach (single-crystal diamond up to 4 inches has been demonstrated on Ir/YSZ/Si) [6, 7]. However, the lattice and thermal expansion mismatches between the substrate and diamond typically result in dislocation densities as high as 10^6-10^8 cm^{-2}, and a stress buffer layer with complex preparation processes is required before diamond growth.

Over the past few decades, extensive efforts have been made to achieve heteroepitaxial diamond on substrates such as Si [7, 8], SiC, TiC, Ni, Pt [9, 10], Co [11], and Ir [12]. Among these materials (Fig. 1), iridium (Ir) has a high melting point, low oxygen permeability, good chemical resistance, and extremely high oxidation resistance, making it a very attractive substrate for diamond heteroepitaxy: (1) It has the same crystal structure as diamond, (2) It has a small lattice mismatch with diamond, approximately 7%, (3) It has no phase transformation and does not form carbides below 1000 °C, (4) It has a high melting point and can form interfacial bonds with carbon, which is favorable for diamond nucleation. However, free-standing epitaxial Ir substrates are difficult to prepare, and bulk Ir single crystals are costly, therefore, alternative substrates suitable for large-area epitaxial Ir growth have been explored. Systems such as Ir/MgO, Ir/YSZ (yttria-stabilized zirconia)/Si, and Ir/STO (strontium titanate)/Si have been studied [7, 8, 13], and diamond films with high crystallinity have been obtained. On YSZ/Si substrates, Schreck et al. grew heteroepitaxial diamond with a diameter of 92 mm and reported a full width at half maximum (FWHM) of the (004) X-ray rocking curve (XRC) of 230 arcsec and a (311) XRC FWHM of 432 arcsec [6, 7]. However, the additional YSZ buffer layer between the diamond/Ir stack and the Si substrate complicates strain control of the diamond layer. In

addition, uniform removal of the Si substrate after diamond growth is extremely difficult. Moreover, MgO and $SrTiO_3$ have much larger thermal expansion coefficients than Ir, making them unsuitable for large-area single-crystal Ir deposition. Compared with other multilayer substrate systems, Ir/Al_2O_3 offers several advantages. Low-cost α-sapphire single crystals are available as high-quality, large-size wafers. In addition, compared with other oxide substrates, the thermal expansion coefficient mismatch between Al_2O_3 and the diamond layer is smaller. In addition, Ir/Al_2O_3 is easier to prepare than the Ir/buffer-layer/Si system.

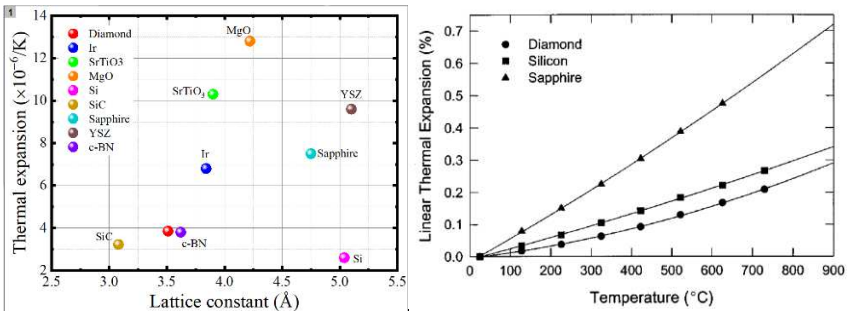


Fig. 1. Relationship between the thermal expansion coefficients and lattice constants of heteroepitaxial substrate materials and diamond (a) and the thermal expansion strain generated within the growth temperature range (b). Reprinted with permission from Ref. [14].

2. Preparation of Ir/Sapphire Composite Substrates

In 2003, Saw et al. directly deposited diamond films on c-plane sapphire substrates by hot-filament chemical vapor deposition (HFCVD) combined with diamond powder grinding [15], using a methane concentration of 1% and a substrate temperature of 850 °C. After 0.5 h of growth, almost the entire surface was covered, from the maximum grain size, the lateral growth rate was estimated to be approximately 3 μm/h, with a nucleation density of approximately 1×10^8 cm^{-2}. After one hour of growth, the polycrystalline diamond film peeled off owing to the large compressive stress between sapphire and diamond. Auger electron spectroscopy revealed no obvious amorphous carbon layer at the interface. Therefore, depositing an Ir transition layer on sapphire is an important basis for achieving diamond heteroepitaxy. Sapphire has a hexagonal crystal structure with lattice constants of a = 0.476 nm and c = 1.299 nm. Ir has a face-centered cubic (fcc) crystal structure with a lattice constant of a = 0.384 nm. Therefore, the growth of Ir on the sapphire surface is essentially heteroepitaxial, and the film quality depends on key factors such as the growth method, growth parameters, substrate surface condition, and post-treatment processes.

Vargas et al. prepared epitaxial Ir on A-plane (11-20), C-plane (0001), and R-plane (01-12) sapphire by metal-organic chemical vapor deposition (MOCVD) and confirmed epitaxial relationships of Ir(100)/sapphire(11-20), Ir(111)/sapphire(0001), and Ir(111)/sapphire(01-12) at substrate temperatures of 500-600 °C [16]. From a crystallographic perspective, Ir on C-plane sapphire should be oriented along the <111> direction because the C-plane offers a small lattice mismatch and three-fold symmetric sites compatible with Ir(111). Although A-plane

sapphire has a large mismatch and crystal asymmetry, studies have demonstrated the epitaxial growth of Ir(100). The group of Golding et al. explored routes to highly stable (001)-oriented Ir films on low-symmetry sapphire planes [17, 18]. To obtain a step-flow surface, (11-20) sapphire substrates (5 × 5×0.5 mm^3) were annealed in a tube furnace in air at 1000-1450 ℃ with different annealing times and heating rates. Annealing at 1450 ℃ for 15 h produced stepped surfaces with single or multiple atomic steps. XRD analysis showed that the crystalline orientation of Ir was directly governed by the substrate temperature during sputtering. At 600 ℃ the films were completely (111)-oriented, whereas more (100) orientation appeared at 700-750 ℃, and the films were almost fully (100)-oriented at 800 ℃ and above. The epitaxial relationship of Ir on A-plane sapphire is not as obvious as that on cubic lattice substrates. The in-plane crystalline orientation relationship between (100) Ir and sapphire is (100) Ir // (11-20) Al_2O_3 and (011) Ir // [1-100] Al_2O_3. On this basis, the same group further investigated the effect of A-plane sapphire substrates with off-cut angles of 0.1°-1° on heteroepitaxial diamond growth[19]. The substrates were annealed in air at 1450 ℃ for 15 h in a tube furnace, and Ir was deposited by electron-beam evaporation at 950 ℃. The annealed sapphire surface showed a stepped morphology, and the surface steps of the substrate with a smaller off-cut angle were wider. Different off-cut angles and processes resulted in different orientations of the Ir film, and (100) or (111) oriented films and their mixtures could be obtained on A-plane sapphire. A substrate temperature threshold of approximately 950 ℃ appears to exist, below which the (100) orientation is unstable. On Ir(001)/Al_2O_3, after 60 min of bias treatment and 5 min of growth, the diamond grains had obviously merged through interface annihilation or overgrowth. After 60 min of growth, a continuous film with a thickness of 0.2 μm was obtained, and almost no voids or grain boundaries were visible on the surface, in contrast to short-time growth.

In 2008, Samoto et al. studied the relationship between the surface morphology of annealed A-plane sapphire substrates and the orientation of the subsequently deposited Ir films [20]. A-plane sapphire substrates were cut into different off-cut (miscut) angles ranging from 0° to 4° along the C-axis (Fig. 2a-2e) and M-axis (Fig. 2f-2i) directions. After annealing in air at 1000 ℃, atomic steps were observed on the substrate surface, and the step width became narrower as the off-cut angle increased. Parallel atomic steps along the C-axis were observed on all substrates miscut towards the C-axis, while the atomic step morphology of the substrates miscut towards the M-axis changed from stripes parallel to the M-axis to complex structures. AFM observations showed that Ir grew epitaxially along the sapphire surface, however, steps or grains larger than those of sapphire were observed, which was attributed to the merging of adjacent Ir grains into larger structures during growth. The FWHM of the Ir rocking curve on the substrate miscut by 4° along the M-axis was larger than that of sapphire, indicating that a higher deposition temperature (>800 ℃) was required to improve the crystallinity of the Ir film. Most areas of the grown diamond film exhibited

the (100) plane, and a flat (100) surface was partially obtained. However, owing to the low nucleation density, the diamond film peeled off rapidly upon cooling.

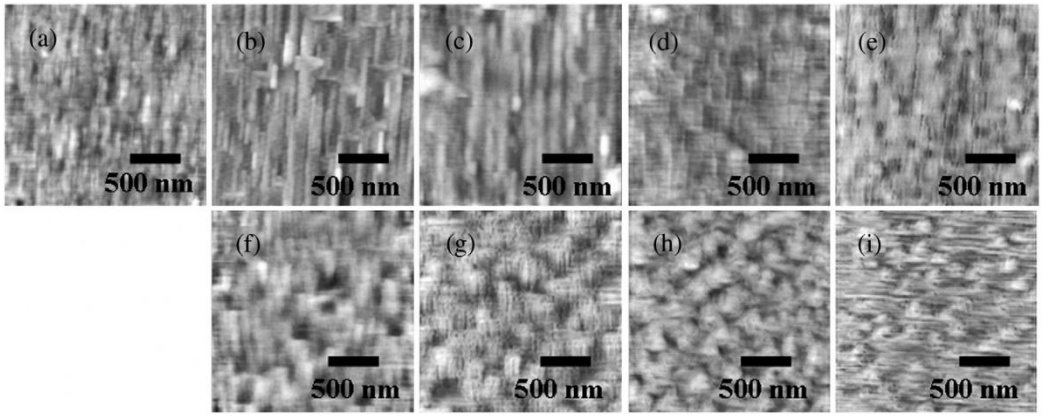


Fig. 2. The images of the surface morphology of the Ir interlayer deposited on A-plane sapphire substrates. The image of (a) shows the surface morphology of Ir on sapphire with a 0° miscut angle. The images from (b) to (e) are of Ir on sapphire with miscut angles (C-axis rotation direction) of 0.5, 1, 2, and 4°, respectively. The images from (f) to (i) are of Ir on sapphire with miscut angles (M-axis rotation direction) of 0.5, 1, 2, and 4°, respectively. Reprinted with permission from Ref. [20].

In 2018, Frank Meyer et al. studied the effect of substrate bias on the growth behavior of Ir films deposited on A-plane sapphire at low substrate temperatures [21]. Three Ir films were deposited on A-plane sapphire (11-20) at 350 ℃: without substrate bias (Sample 1), with substrate bias applied throughout deposition (Sample 2), and by a two-step process (Sample 3). The two-step deposition involved first depositing a thin Ir layer (approximately 20 nm) with additional substrate bias, and then continuing to deposit Ir to a total thickness of approximately 300 nm with the substrate bias turned off. The film grown without bias exhibited a predominantly (111) texture. The Ir film deposited with continuous substrate bias showed a more uniform morphology composed of small grains, with significantly improved crystallinity and an increased proportion of (001)-oriented crystallites. The two-step process yielded a flat surface dominated by (001) out-of-plane-oriented grains. However, the FWHM of the rocking curve of the Ir (002) peak was approximately 3 to 4 times that of the film deposited at 600 ℃ reported in the literature. The applied bias raised the potential energy of all particles arriving at the surface and markedly increased the kinetic energy of bombarding ions, enhancing the surface mobility of adatoms and promoting the evolution of well-oriented Ir nuclei. Excessive substrate bias hindered lateral growth, introduced defects in the growing film, and impeded the coalescence of crystallites, so that only partial epitaxial growth could be observed.

In 2022, Wang et al. from Harbin Institute of Technology studied the role of surface chemistry in determining the heteroepitaxial growth of Ir films on a-plane sapphire single crystals [22]. A 2-inch (11-20) sapphire wafer was cut into 10 × 10 × 0.5 mm^3 pieces, which were pretreated by different processes-annealing in air (1300 ℃, 24 h), in-situ Ar^+ ion etching (5 min), solvent cleaning, and Ar^+ ion etching-to study their effects on Ir sputtering. The substrate

temperature during Ir film sputtering was 800 °C, and the deposition rate was 0.035 nm/s. For the untreated and air-annealed samples, a strong Ir (111) peak and a very weak Ir (002) peak were observed. In contrast, only the Ir (002) diffraction peak was detected in the Ar^+-etched samples, and azimuthal scans revealed the four-fold symmetry of the Ir (001) plane. This indicates that Ar^+ ion etching is more effective than annealing in promoting Ir (002) film growth on (11-20) sapphire substrates. After annealing in air at 1300 °C for 24 h, a stepped morphology was observed. The strong interaction between the epitaxial material and the step edges significantly reduces the nucleation barrier, and the nucleation and growth of Ir films usually start from the step edges and have a stepped morphology. However, during annealing, the surface undergoes a passivation reaction (forming AlO_2 species) and accumulates carbon adsorbates. Surface reconstruction and contamination weaken the interaction between Ir adatoms and the substrate, reducing adatom mobility and favoring growth on the lowest-surface-energy (111) plane. The clean surface produced by Ar^+ etching exposes substrate dangling bonds, enhancing Ir-substrate interactions and promoting epitaxial growth of Ir (002).

In 2026, Uwihoreye et al. from Xiamen University grew high-quality Ir films with controllable crystal orientations on a-plane sapphire substrates by adjusting the annealing temperature [23]. By designing a 7° off-cut angle along the [1-100] direction on a-plane Al_2O_3(11-20) substrates, a vicinal surface with a high step density and narrow terraces was formed. This step-terrace configuration not only provides nucleation sites but also acts as a distributed strain relaxation network during heteroepitaxial growth. Annealing the clean substrate in air at 900 °C for 30 min preserved the step-terrace structure. The straight step edges provide preferential nucleation sites for Ir adatoms, while the confined terraces limit the adatom diffusion length below the island-nucleation threshold, promoting step-edge incorporation and finally yielding high-quality Ir(100) films with pronounced step-flow growth. During annealing at the higher temperature of 1100 °C, the large off-cut angle induces strong step coalescence, producing widened terraces, curved steps, and a faceted morphology with serrated step edges. This “valley” morphology limits the migration of adatoms and enhances secondary nucleation, thereby stabilizing three-dimensional growth. As mentioned earlier, this growth is consistent with the surface energy hierarchy characteristic of face-centered cubic metals ($\gamma_{111} < \gamma_{100} < \gamma_{110}$), enabling Ir to nucleate in the thermodynamically favorable (111) orientation. Through island merging, highly textured Ir(111) films are obtained. Therefore, by changing the thermal annealing conditions of the sapphire substrate to induce surface reconstruction and step rearrangement, Ir(100) and Ir(111) films can be selectively deposited under otherwise identical experimental conditions (Fig. 3).

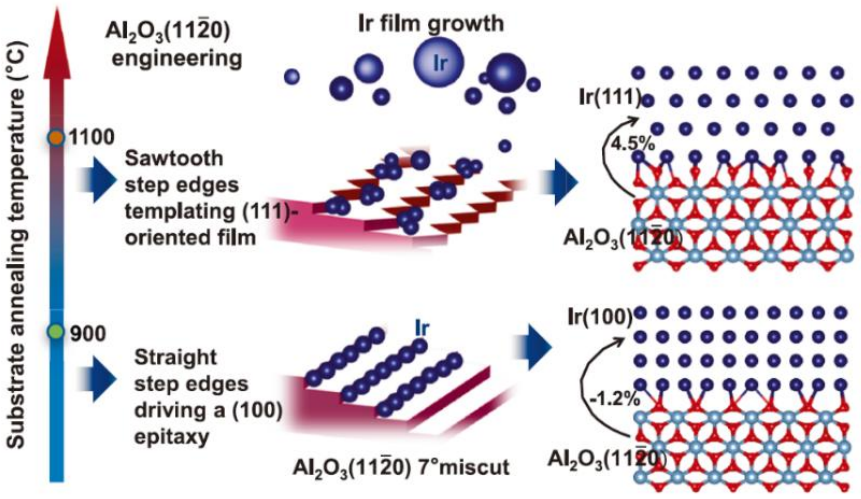


Fig. 3. Schematic representation of sapphire surface engineering through thermal annealing, with corresponding Ir growth and atomic representation. Reprinted with permission from Ref. [23].

3. Progress in Heteroepitaxial Growth of (001) Single-Crystal Diamond Materials

From the development history of diamond semiconductors, the (100) plane has many advantages over non-(100) planes in terms of large-size, low-defect-density growth and polishing. After years of exploration, the growth of (100)-plane diamond has become more mature, and heteroepitaxy has consequently made significant progress on this plane first. In 2020, Kim et al. from Saga University successfully grew a 1-inch free-standing (001) diamond layer on (11-20) a-plane sapphire substrates with an Ir buffer layer using the microneedle method (Fig. 4) [24]. An approximately 1-μm-thick Ir buffer layer was deposited on (11-20) sapphire (α-Al_2O_3) substrates with an orientation deviation of less than 0.15°. After bias-enhanced nucleation to promote diamond nucleation, the diamond layer was grown by microwave plasma CVD (growth rate of 6 μm/h). The diamond layer was selectively etched through a Ni mask to form vertically aligned columnar structures, the so-called microneedles [25]. The height of the diamond microneedles was 50 μm, the diameter was 2 μm, and the spacing was 10 μm. A diamond layer 800-1000 μm thick was then continuously grown on the microneedles at 16.6 μm/h. The microneedles release the high residual strain caused by the CTE mismatch between the Ir/sapphire substrate and diamond. During post-growth cooling, the diamond layer spontaneously peeled off from the Ir/sapphire substrate at the microneedles, without generating cracks. X-ray pole figure measurements showed four-fold symmetry, indicating that the layer was a single crystal free of twins. The epitaxial relationship was determined as diamond(001)[110] ∥ Ir(001)[110] ∥ sapphire(11-20)[0001]. The dislocation density of the diamond layer was determined to be 1.4×10^7 cm^{-2} by plan-view transmission electron microscopy. In addition, the curvature radius of the diamond layer was 90.6 cm, much larger than the previously reported value of approximately 20 cm. The wafer did not crack or break after growth and polishing processes.

However, the wafer broke into three pieces during photolithographic mask patterning for diamond FET fabrication. The fabricated FET exhibited a breakdown voltage of 618 V, a drain current of 505 mA/mm, a specific on-resistance of 2.63 mΩ·cm^2, and a Baliga's figure of merit (BFOM) of 145 MW/cm^2.

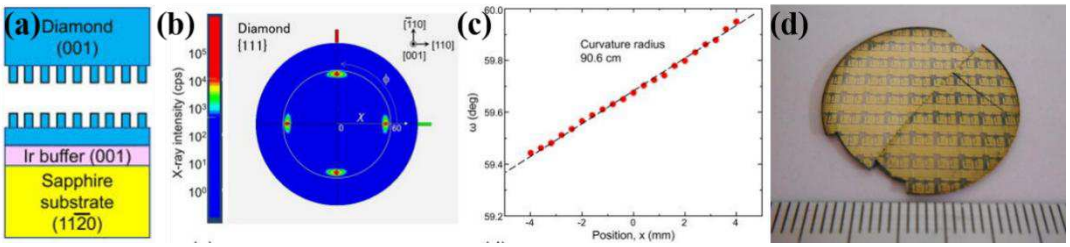


Fig. 4. Heteroepitaxy of diamond on sapphire using the microneedle structure: (b, c) X-ray pole figure and (004) diffraction at different positions, (d) photograph of the 1-inch free-standing heteroepitaxial diamond after photolithography. Reprinted with permission from Ref. [24].

Because of the high elastic modulus (538.3 GPa), high rigidity, and strong brittleness of Ir, large stresses are generated upon straining, when Ir is used as a buffer layer on oxide substrates, it is prone to peeling and even fracture, which is detrimental to heteroepitaxial single-crystal diamond growth. In 2021, the group of Hongxing Wang at Xi'an Jiaotong University introduced a Pd layer between Ir and Al_2O_3(11-20) as a support/buffer layer [26]. Pd has good ductility and plasticity, and its elastic modulus (≈121 GPa) is much lower than that of Ir (≈528 GPa). In addition, Pd has a face-centered cubic structure similar to that of Ir and a close lattice constant (3.84 Å for Ir vs. 3.89 Å for Pd). In addition, Pd has a high melting point (1554 °C). Therefore, using Pd as a buffer layer between Ir and the oxide substrate can effectively reduce the stress in heteroepitaxial diamond growth. SEM results showed that the deposition quality of the Ir film improved significantly with increasing Pd thickness, and the FWHM of the Ir (002) rocking curve was reduced by 26% compared with that of the pure Ir film. After 70 h of growth, a heteroepitaxial diamond single-crystal film of 20 × 20 × 0.6 mm^3 was obtained. The FWHMs of the (004) and (311) rocking curves were 194 and 396 arcsec, respectively (Fig.5a and 5b). Raman spectroscopy showed a strong diamond peak at 1332 cm^{-1} (Fig.5c). XRD reciprocal space mapping showed that most of the diffraction intensity was located near the bulk Bragg position, confirming that the diamond layer was essentially relaxed (Fig 5d and 5e). Typical single-crystal diamond step features were visible under an optical microscope (Fig. 5f and 5g).

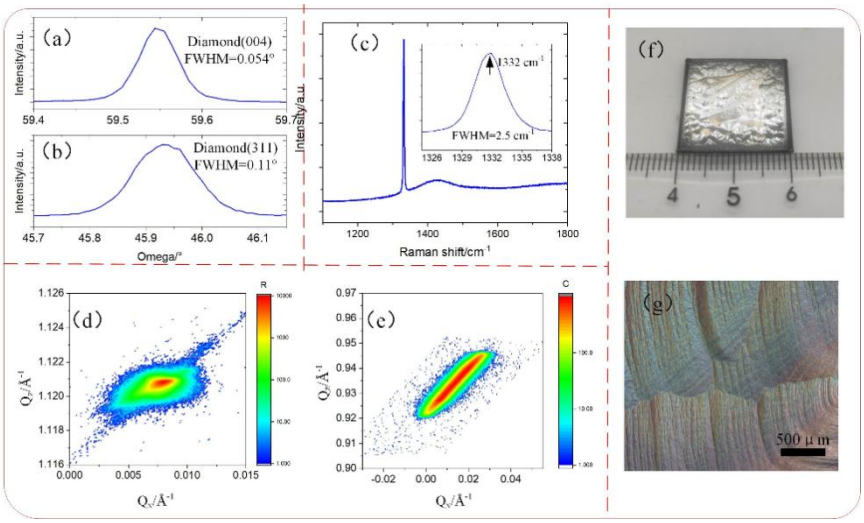


Fig. 5. (a,b) ω-scan XRD rocking curves of the (004) and (311) reflections, (c) Raman spectrum, (d,e) reciprocal space maps of the (004) and (311) reflections, (f) photograph of the obtained diamond single crystal, (g) optical microscope image. Reprinted with permission from Ref. [26].

In 2021, Kim et al. used off-cut substrates to promote step-flow growth, thereby effectively regulating the residual stress in the diamond layer and achieving 2-inch single-crystal diamond [27]. Off-cut angles of (11-20) sapphire (α-Al_2O_3) varied from 0° to 7°, with off-cut directions along the [1-100] m-axis or the [0001] c-axis. An approximately 1-μm-thick Ir buffer layer was deposited on the sapphire substrate by sputtering. After bias-enhanced nucleation (BEN) treatment of the Ir buffer layer, diamond was grown at a rate of 16.5 μm/h. During cooling, the sapphire substrate shrank more than the diamond layer, and the 2-inch diamond layer together with the Ir buffer layer spontaneously peeled off from the sapphire substrate without cracking (Fig. 6a). X-ray diffraction results showed that even with off-cut sapphire substrates, the diamond (001) layer and the Ir (001) buffer layer still epitaxially grew along the sapphire [11-20] direction. The FWHMs of the diamond (004) and (311) reflections decreased significantly as the off-cut angle increased towards the [0001] or [1-100] direction, indicating improved crystal quality. The lowest FWHM was obtained at an off-cut angle of 7° along the m-direction (Fig. 6b). For substrates without an off-cut, catastrophic cracking occurred during post-growth cooling owing to residual stress. In contrast, for off-cut substrates, the extent of sapphire cracking decreased with increasing off-cut angle. The curvature radii of the diamond layer along the substrate [1-100] and [0001] directions were 99.64 and 260.21 cm, respectively. The dislocation density was 2.6×10^7 cm^{-2}.

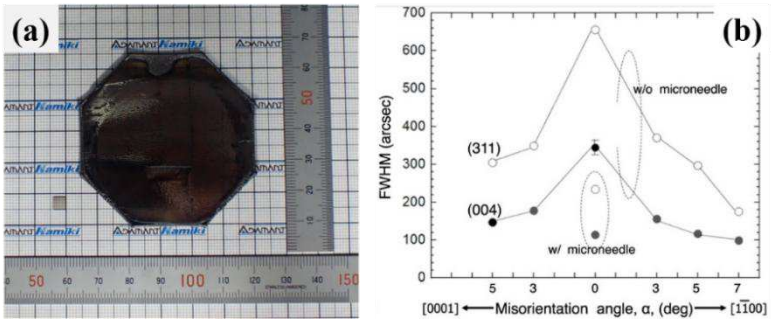


Fig. 6. (a) Photograph of the 2-inch as-grown free-standing heteroepitaxial diamond wafer, (b) misorientation-angle dependence of the FWHM of the diamond (004) and (311) XRC peaks for [0001] c- and [1-100] m-misorientation directions. Reprinted with permission from Ref. [27].

Currently, mainstream diamond growth equipment is based on 2.45 GHz MPCVD, whose power is generally limited to 15 kW with an effective deposition diameter of approximately 80 mm-insufficient to meet the growing demand for larger diamond diameters. 915 MHz MPCVD can achieve deposition sizes of 8 inches or more. However, the plasma density at similar power levels is relatively low. The (100) surface of diamond has extremely high surface energy, making it difficult to nucleate on non-diamond substrates without special treatment. Therefore, whether 915 MHz microwave plasma can be used for DC-BEN heteroepitaxy of diamond on Ir remained an open question. In 2026, Tzeng et al. studied the bias-enhanced nucleation process on Ir(100)/a-sapphire using 915 MHz MPCVD [28]. A high-quality (100) Ir film was deposited on a single-side-polished 2-inch a-plane sapphire substrate at 900 ℃. At a bias voltage of -250 V, the Ir(100) surface exhibited a shallow groove-like structure with a specific orientation, and approximately 1-μm amorphous carbon (a-C) spherical aggregates were sparsely distributed. When the negative bias voltage was increased to -270 V and -290 V, a clear domain structure appeared, forming a continuous a-C interlayer. After 60 min of growth, a locally continuous diamond film formed on the sample surface. Extending the BEN time to 30 min significantly improved the nucleation density, and the center of the sample was covered by an almost continuous (100)-textured diamond layer. When the BEN time was further increased to 45 min, although the domain coverage increased, excessive carbon injection triggered secondary nucleation on the epitaxial grains and degraded the overall orientation.

A significant limitation of traditional DC bias-enhanced nucleation (BEN) is the requirement for a conductive path for the biased ion current to flow from the plasma to the negatively biased substrate holder. For insulating sapphire substrates, the bias current flows from the plasma to the Ir surface and laterally through the Ir film to the edge of the substrate, and finally into the substrate holder. The voltage drop along this resistive current path leads to non-uniform ion bombardment energy and flux on the Ir film, especially for large substrates with diameters of 6-12 inches. In 2026, Tzeng et al. employed radio-frequency bias-enhanced nucleation (RF-BEN) to achieve

heteroepitaxial nucleation of (100) diamond on a-sapphire [29]. Because electrons diffuse much faster than ions, the plasma always acquires a positive potential relative to the surrounding solid surfaces, hence, the substrate potential is negative relative to the plasma. At low RF powers (40 W, 60 W), the ion energy of carbon species was insufficient: only spherical and island-like aggregates formed on the surface, and no diamond nucleation occurred. When the RF power was increased to 100-120 W, grooves and plow grooves arranged along the [110] direction appeared on the surface, but the diamond nuclei mainly existed as ultra-thin "domain"-type carbon overlayers without visible grain features in SEM. When the methane concentration exceeded 8%, white dendritic regions were sparsely distributed on the groove/plow-groove network. Further increasing the methane fraction significantly expanded the domain coverage, but the excessive carbon supply produced many aggregates on top of the domains.

4. Progress in Heteroepitaxial Growth of (111) Single-Crystal Diamond Materials

Significant progress has been made in the heteroepitaxial growth of (100) single-crystal diamond, which has become the main platform for wafer-level diamond technology. In contrast, heteroepitaxial growth along the (111) orientation is still in its early stage, because (111)-plane diamond is prone to twinning and non-diamond phase defects during growth, resulting in inferior crystalline quality and low carrier mobility. Nevertheless, (111)-oriented diamond offers unique advantages, including higher n-type doping efficiency, higher two-dimensional hole gas (2DHG) densities achievable by surface doping, and better compatibility with nitride semiconductors for hybrid integration. The n-type doping concentration and doping efficiency of the (111) plane are 1-2 orders of magnitude higher than those of the (100) plane. SBDs fabricated on (111) diamond, or p-n diodes (PNDs) obtained by sequential p- and n-type growth, exhibit good electrical characteristics. In addition, NV color centers in (100) diamond have four possible lattice orientations, whose random distribution disperses the signal intensity and reduces detection efficiency. In (111)-grown diamond, more than 97% of the NV centers can be aligned along the [111] direction, which effectively improves the sensitivity of quantum sensing systems. These characteristics make (111) heteroepitaxial diamond a very attractive candidate for future electronic device applications. However, research progress is limited by the available size of non-(100) single-crystal diamond wafers. Shimaoka et al. grew an HPHT (100) substrate to $10 \times 10 \times 6$ mm^3, cut out a (111) seed crystal of 7×6 mm^2, and envisioned scaling up by a cloning-stitching method [30]. However, this method involves complex processes, and suppressing defects at the stitching seams is more difficult than for the (100) plane. Research on the heteroepitaxial growth of (111)-plane diamond films has a long history, and significant breakthroughs have been made in recent years.

Previous studies have shown orientation relationships of diamond(111) ∥ Pt(111) and diamond(110) ∥ Pt(110) between diamond and Pt, and diamond films heteroepitaxially grown on Pt(111) exhibit smooth (111) surfaces with

spontaneous coalescence and excellent in-plane azimuthal alignment. In 1999, Tachibana et al. studied the growth of (111)-oriented diamond films on sputter-deposited Pt(111) epitaxial films on sapphire(0001) single crystals [9]. A 4-μm Pt film was deposited on mirror-polished sapphire(0001) by DC magnetron sputtering at 600 ℃. XRD patterns showed that the Pt film was mainly (111)-oriented on the sapphire(0001) substrate. Ex-situ reflection high-energy electron diffraction (RHEED) observations also confirmed the epitaxial relationship between Pt and sapphire: Pt(111) ‖ sapphire(0001), Pt(110) ‖ sapphire(010). The morphology of the 1.5-μm-thick (111) diamond film showed that, although randomly oriented grains existed in some surface areas, many (111)-oriented crystals coalesced, and the unmerged regions also exhibited a high degree of (111) orientation with good azimuthal alignment. SEM images clearly revealed two epitaxially oriented diamond variants differing by 60° in azimuth. The XRD rocking-curve FWHM was approximately 2.0°, confirming the structural quality of the diamond film. However, Pt significantly absorbs hydrogen and hydrocarbons in the CVD environment, hindering diamond nucleation. Hydrocarbons diffuse through Pt and form a graphite layer at the Pt/sapphire interface, resulting in poor adhesion and damage of the diamond film. Sawabe's group showed that the low solubility of carbon and hydrogen in Ir favors the formation of highly oriented diamond [12]. A Pt(111)/Ir(111)/Pt(111) stack was sputtered on (0001) sapphire substrates (10 × 10 mm^2) at 600 ℃ and annealed in vacuum at 900 ℃ [10]. The sputtered Pt layer was highly oriented, with a rocking-curve FWHM of 0.16°. Diamond was grown by MPCVD, with a methane concentration of 0.3% and a temperature of 875 ℃. The 1.5-μm diamond film showed obvious triangular grains, together with many randomly oriented grains. The rocking-curve FWHM was approximately 1.1°. The Ir layer effectively prevented carbon diffusion into Pt, enhancing the nucleation of oriented diamond on the substrate surface. It also inhibited graphite formation between Pt and sapphire, thereby improving diamond adhesion, as evidenced by the color of Pt visible through the transparent sapphire substrate [10].

Ruthenium (Ru) has a hexagonal structure, yet its physical and chemical properties are similar to those of Ir, which has been widely studied for diamond heteroepitaxy. For example, their melting points (Ru: 2334 ℃, Ir: 2466 ℃) and the lattice mismatches of their in-plane hexagonal atomic arrangements with diamond (111) (Ru(0001): 6.9%, Ir(111): 7.3%) are comparable. The low chemical activity of hexagonal Ru makes it a potential substrate for (111) diamond deposition. Moreover, the price of Ru is only one-quarter that of Ir, making it a cost-effective candidate for producing large-size single-crystal diamond substrates [31]. A 150-nm Ru layer was sputtered onto C-plane sapphire substrates (5 × 5×0.5 mm^3) in two steps at 600 ℃: first with a bias voltage of -50 V and then without bias. Microwave plasma bias nucleation was performed at -150 V and 650 ℃ for 30 s with a methane concentration of 10%. The subsequent growth temperature was approximately 600 ℃, and the methane concentration was 0.3%.

XRD showed that Ru exhibited six-fold symmetry with a (0001) orientation at 60° intervals. Diamond grown for 30 min showed (111) grains with a double orientation flipped by 180°. However, the diamond formed islands with a diameter of 500 nm and did not coalesce into a continuous film.

Motivated by the success of (100)-plane heteroepitaxy, research has also been extended to (111) diamond heteroepitaxial growth on Ir surfaces. Choi et al. (Nam's group) prepared sapphire substrates of 10 × 10 mm^2 with (11-20) and (0001) orientations (without off-cut) [32]. An approximately 900-nm-thick Ir layer was deposited by sputtering at 850 ℃, followed by bias-enhanced nucleation and MPCVD growth of diamond. XRD 2θ-ω measurements showed that both diamond and Ir grew along (001) on (11-20) sapphire, whereas both grew along (111) on (0001) sapphire. In addition, a diffraction peak corresponding to iridium oxide formed during the initial growth stage was observed on (0001) sapphire (Fig. 7). φ-scan azimuthal measurements showed four-fold symmetry for the (001) diamond/(001) Ir/(11-20) sapphire system, whereas the (111) diamond/(111) Ir/(0001) sapphire system exhibited six peaks owing to 180° twin boundaries. In the (001) Ir/(11-20) sapphire system, the lattice mismatch was -1.2% along [1-10] Ir ‖ [1-100] sapphire and 4.5% along [110] Ir ‖ [0001] sapphire. In contrast, in the (111) Ir/(0001) sapphire system, the lattice mismatches along [1-10] Ir ‖ [1-100] sapphire and [-1-12] Ir ‖ [11-20] sapphire were -5.3% and 7.5%, respectively, because Ir atoms interacting with the surface oxygen of sapphire encounter two different O-O bond distances (2.52 and 2.87 Å). Moreover, this fcc metal is prone to forming 180° rotation twins along the [111] axis perpendicular to the growth surface. Cross-sectional TEM showed that the high-density defects formed at the (001) diamond/Ir interface were almost eliminated within the first micrometer of growth. However, the defect-elimination rate at the (111) diamond interface was low, and selected-area electron diffraction (SAED) revealed twin diffraction rotated by 180° about the growth axis. This is because the Ir surface grown on (11-20) sapphire exhibits an elongated square structure, with BEN-generated ridges and grooves oriented along [-110] and [110]. After 60 s of MPCVD growth, the surface was completely covered by diamond grains. The Ir surface grown on (0001) sapphire exhibited hexagonal mounds. After BEN treatment, no preferred ridge/groove orientation was observed, but irregularly distributed pits formed on the roughened Ir surface. The (111) diamond surface grown for 1500 s was severely roughened, with upward- and downward-oriented triangular morphologies. Although these studies represent key milestones, the formation of twin domains remains an inherent challenge in the growth of (111) diamond on sapphire substrates.

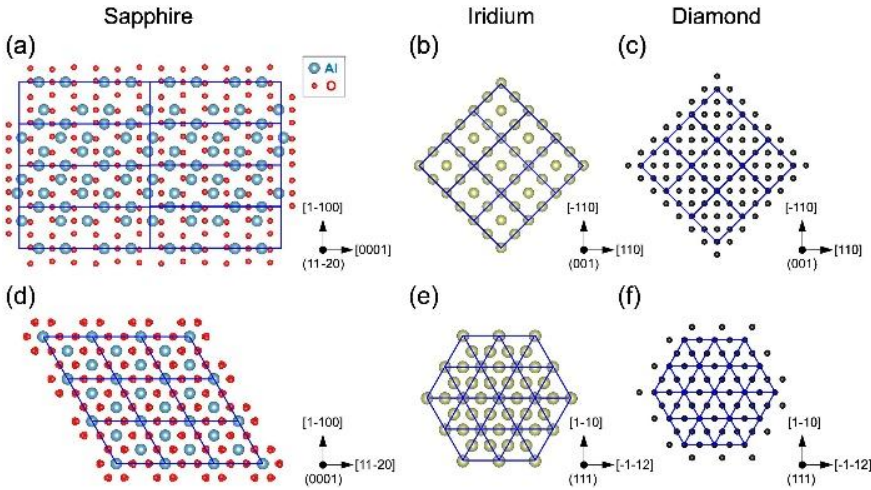


Fig. 7. Atomic structures of sapphire, iridium, and diamond. (a) and (d) represent the atomic arrangements of (11-20) and (0001) sapphire, respectively. Blue and red dots represent Al and O atoms, respectively. (b) and (e) represent the atomic arrangements of (001) and (111) Ir, respectively. (c) and (f) represent the atomic arrangements of (001) and (111) diamond, respectively.Reprinted with permission from Ref. [32].

In 2025, Kwak et al. systematically studied and compared the growth behavior, twin characteristics, and formation mechanisms of diamond (111)/Ir(111) films on r-plane and c-plane sapphire substrates [33]. Commercial r-plane and c-plane sapphire substrates of 10 × 10 × 0.43 mm^3 were used, Ir(111) layers were sputtered at 750-780 ℃, with rocking-curve FWHMs of 0.3° and 0.27°, respectively. 2θ-ω X-ray diffraction showed out-of-plane epitaxial relationships of diamond(111) ‖ Ir(111) ‖ sapphire(0001) and sapphire(1-102), respectively. The multi-domain nature of the Ir(111) layer on c-plane sapphire promoted partial oxidation of the Ir surface, forming IrO_2. φ-scan azimuthal measurements showed only one diffraction peak for the r-plane sapphire substrate, reflecting single-fold rotational symmetry arising from its tilted surface within the trigonal lattice. The Ir(111) layer on r-plane sapphire was single-domain with clear three-fold symmetry. Similarly, diamond(111) showed diffraction peaks at the same φ values as Ir(111), indicating that the diamond layer inherited the same lattice orientation. The c-plane sapphire substrate showed six diffraction peaks owing to its trigonal structure, and the corresponding Ir(111) layer also exhibited six diffraction peaks (Fig. 8). Diamond(111) showed peaks at the same φ positions, indicating that the twinned diamond layer maintained the same epitaxial relationship with the underlying twinned Ir(111) film. The Ir(111) film grown on r-plane sapphire showed a featureless, smooth surface (Fig. 9a), whereas clear grain boundaries were observed in the Ir(111) layer on c-plane sapphire (Fig. 9b). After 60 min of diamond growth, a uniform, single-domain diamond(111) film was obtained on Ir(111)/sapphire(1-102) (Fig. 9c), whereas diamond growth on Ir(111)/sapphire(0001) followed the grain boundaries shown in Fig. 9b (Fig. 9d). The (111) diamond film grown on r-plane sapphire for 60.5 h reached a thickness of 21.5 μm and spontaneously delaminated during cooling. The rocking-curve FWHMs of the (111) and (311) reflections were 0.55° and 0.23°, respectively.

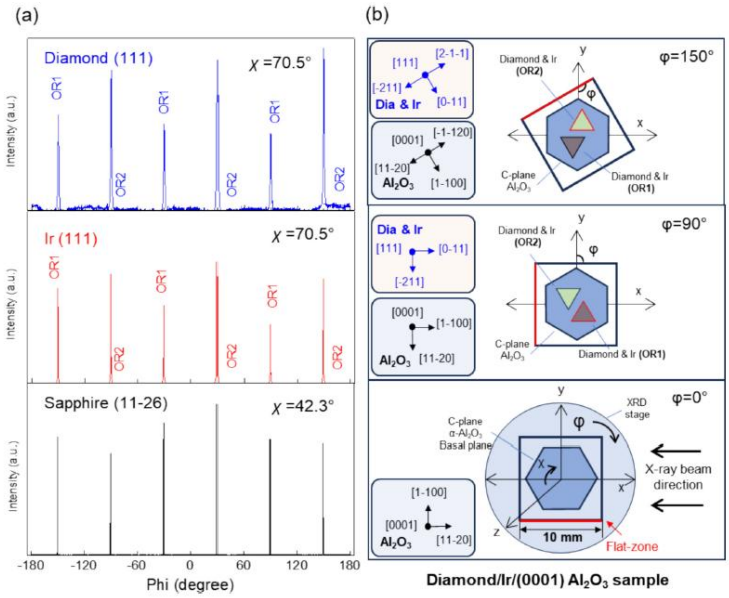


Fig. 8. (a) φ-scan (azimuthal) X-ray diffraction patterns of diamond/Ir/c-plane sapphire, (b) schematic diagrams of the epitaxial orientation relationships between the diamond and Ir layers. Reprinted with permission from Ref. [33].

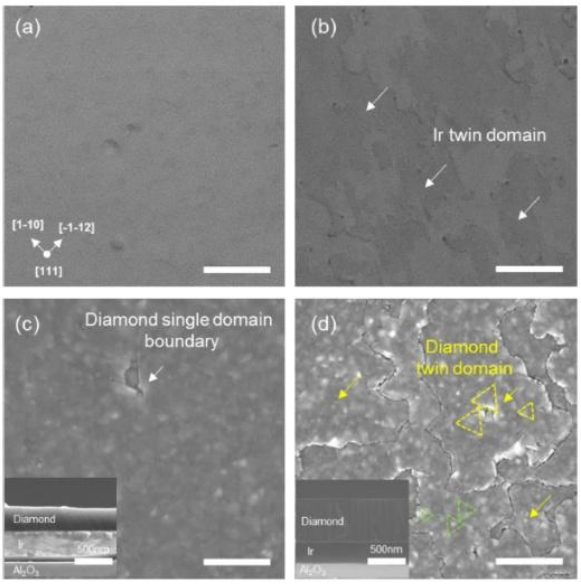


Fig. 9. SEM plan-view images of the Ir(111) layers deposited on r-plane and c-plane sapphire substrates before and after 60 min of diamond growth. Reprinted with permission from Ref. [33].

In 2026, Kim et al. investigated the effect of off-cutting (0001)-plane sapphire substrates towards the (11-20) a-axis or the (-1010) m-axis by 0.2°-14° on heteroepitaxial (111) diamond growth [34]. When the off-cut angle towards (11-20) was ≥7°, triangular patterns arranged along the (11-2) direction appeared on the diamond surface, reflecting the stable step structure of (111) diamond. At an off-cut angle of 0.2°, six-fold symmetry was observed, whereas all other off-cut angles showed three-fold symmetry, indicating the absence of twins. In contrast, when the (0001) sapphire was off-cut towards (-1010), stepped surface features were observed and the pole figure showed six-fold symmetry, indicating the presence of twins. When the (0001) sapphire is off-cut towards the (11-20) a-axis, the off-

cut direction coincides with the stable step-flow direction of [111] diamond, i.e., the (11-2) direction. Step-flow growth is therefore promoted, and the apex direction of the triangular steps is aligned with the step-flow direction, thereby inhibiting twin formation. When off-cut towards the m-axis, two types of triangular steps rotated by 60° relative to each other, or steps rotated by 180°, are stably formed, leading to twin formation. Furthermore, a free-standing transparent (111) diamond film approximately 300 μm thick was obtained on a 30 mm square (0001) c-plane sapphire substrate (Fig. 10a and 10b). The X-ray (220) pole figure showed three-fold symmetry without additional twin peaks (Fig. 10c). The (111) rocking-curve FWHM was 94 arcsec and the Raman peak FWHM was 2.72 cm^{-1}, indicating excellent crystalline quality of the heteroepitaxially grown diamond (Fig. 10d and 10e). Very weak blue luminescence was observed from the top surface, while relatively strong blue luminescence was observed from the side surface (Fig. 10f).

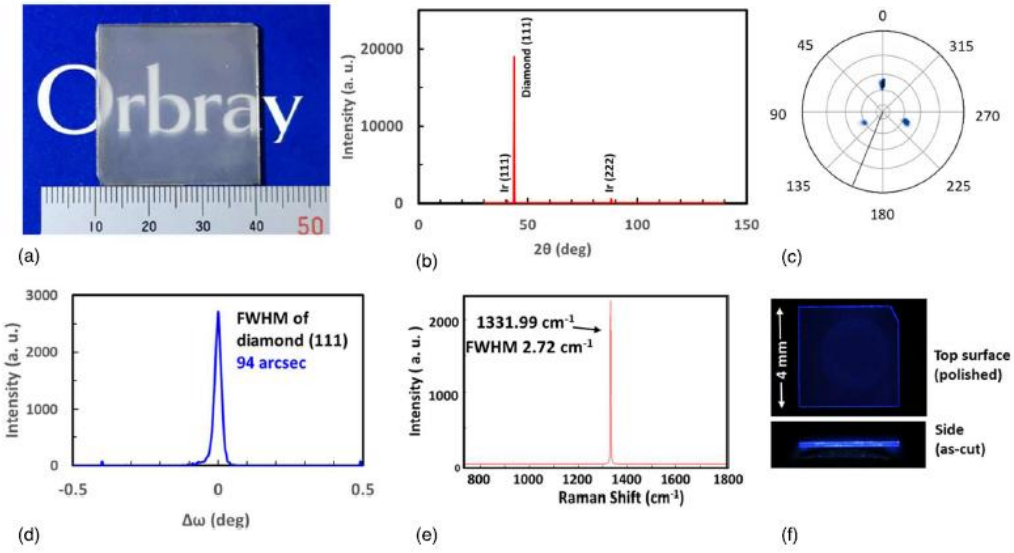


Fig. 10. Representative characterization results of a 30 mm square free-standing (111) diamond film grown on a (0001) c-plane sapphire substrate off-cut towards the (11-20) a-axis: (a) photograph of the representative free-standing diamond film, (b) XRD 2θ-ω scan, (c) (220) pole figure, (d) X-ray rocking curve, (e) Raman spectrum, (f) PL image recorded under ultraviolet light excitation. Reprinted with permission from Ref. [34].

5. Device Applications of Heteroepitaxial Single-Crystal Diamond Materials

In 2021, Kwak et al. realized quasi-vertical Schottky barrier diodes (SBDs) on free-standing diamond heteroepitaxially grown on sapphire substrates (Fig. 11a) [35]. A heavily boron-doped p^+ layer 1 μm thick (1×10^{20} cm^{-3}) was grown to reduce the contact resistance and facilitate current spreading, and an unintentionally doped p^- drift layer 1 μm thick (1×10^{16} cm^{-3}) was grown using reactor residuals. A 300-nm-thick aluminum layer was deposited as an etching mask, and etching towards the substrate was performed using an O_2/Ar gas mixture. Ti/Au (50/100 nm) was deposited and annealed at 500 °C for 1 h in argon to form ohmic contacts. Aluminum Schottky

electrodes with a diameter of 100 μm and a thickness of 100 nm were deposited and patterned by a lift-off process. Although heteroepitaxial diamond substrates of the same quality were used, the number of surface defects in the diamond SBD increased with the methane flow rate. When surface defects were located within the Schottky electrode region (Fig. 11b), stepped I-V curves with large forward leakage currents were observed. The ideality factor was 1.4 and the maximum breakdown field was 1.1 MV/cm, indicating that the high dislocation density in the heteroepitaxial diamond epitaxial layer limited the breakdown field to well below the theoretical value. Most threading dislocations in the SBD epitaxial layer grown on heteroepitaxial diamond substrates were of the 45° mixed type (Fig. 11c), causing premature breakdown or large leakage and degrading device performance [35].

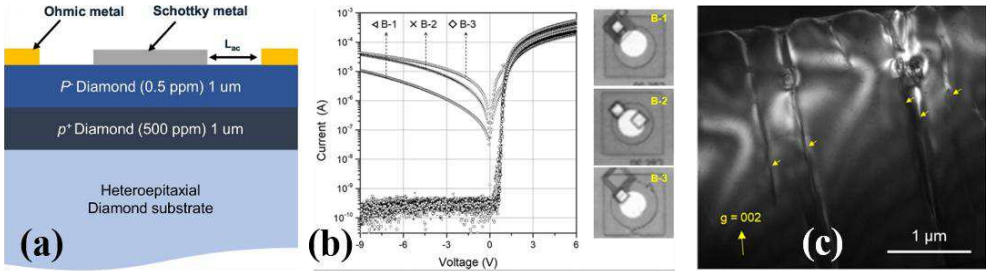


Fig. 11. Diamond Schottky barrier diode: (a) schematic structure, (b) current-voltage characteristics, (c) cross-sectional TEM dark-field image. Reprinted with permission from Ref. [35].

In 2022, the group of Hongxing Wang realized hydrogen-terminated surface-channel MOSFETs on 1-inch heteroepitaxial single-crystal diamond [36]. An approximately 150-nm-thick Ir layer was sputtered onto (11-20) sapphire substrates (26 × 26 × 1 mm^3) at high temperature, followed by BEN and MPCVD growth. The FWHM of the (004) X-ray rocking curve was 209.52 arcsec. Hydrogen plasma treatment for 20 min formed a surface two-dimensional hole gas (2DHG) channel, and a two-step atomic layer deposition (ALD) process was used for the Al_2O_3 passivation layer: a 5-nm Al_2O_3 layer was first deposited at 90 ℃ to protect the C-H bonds from oxidation, followed by a 25-nm Al_2O_3 layer at 250 ℃. At VGS = -8 V and VDS = -30 V, the maximum current density was 172 mA/mm, the on-resistance (*Ron*) was approximately 130.5 Ω·mm, and the maximum transconductance (gm,max) was 10.4 mS/mm. The threshold voltage (Vth) was deduced to be 11.85 V, showing normally-on characteristics. The fixed negative charge density, trap charge density, and interface state density were calculated from the flat-band voltage, flat-band voltage hysteresis, and subthreshold swing to be 1.66 × 10^{13} cm^{-2}, 4.03 × 10^{12} cm^{-2}, and 1.07 × 10^{13} eV^{-1} cm^{-2}, respectively. After annealing in N_2 at 423 K for 3 min, the maximum effective field-effect hole mobility (μeff) increased by 27%. In contrast, when the annealing temperature was raised to 473 K, Dit increased sharply and μeff decreased sharply, indicating that the annealing temperature and time must be precisely controlled to preserve the quality of the Al_2O_3/diamond interface.

Kasu et al. reported high-performance diamond metal-oxide-semiconductor field-effect transistors (MOSFETs) on heteroepitaxial diamond substrates [37]. The diamond substrate was grown on an off-cut sapphire substrate by the step-flow method, followed by homoepitaxial growth of an approximately 100-nm-thick intrinsic diamond layer. The sample was exposed to 2% NO_2 gas (diluted in N_2) for p-type doping to maintain a high-density 2DHG channel. A 16-nm-thick Al_2O_3 bilayer was deposited by ALD to passivate the active channel and serve as the gate insulator. First, a 4-nm layer was deposited at 120 °C to minimize NO_2 desorption during sample heating, then, a 12-nm layer was deposited at 230 °C to improve the overall Al_2O_3 quality. At VGS = -7 V and VDS = -40 V, the MOSFET exhibited a maximum drain current density (ID) of 372 mA/mm (Fig. 12a). The threshold voltage (Vth) obtained by linear extrapolation was 4.1 V, and the interface state density (Dit) was 4.6×10^{12} eV^{-1} cm^{-2} (Fig. 12b). For a MOSFET with LGD = 50 µm, the DC output current density was 83 mA/mm, and *Ron* was 478 Ω·mm (Fig. 12c). In the off-state (VGS = 7 V), the MOSFET broke down at a drain voltage of 3659 V-the highest breakdown voltage reported for diamond MOSFETs to date (Fig. 12d).

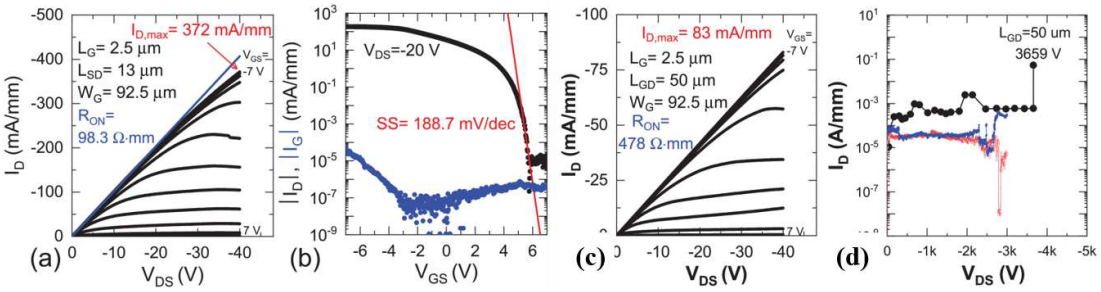


Fig. 12. (a,b) Output and gate current characteristics of the diamond MOSFET, (c,d) output and off-state current characteristics of a MOSFET with LGD = 50 µm. Reprinted with permission from Ref. [37] @2023 IEEE.

In 2026, Zhu et al. from Harbin Institute of Technology realized a free-standing heteroepitaxial single-crystal diamond film with a (001) surface orientation on a 20 × 20 mm^2 Ir/Al_2O_3 composite substrate and fabricated ultraviolet photodetectors [38]. To reduce threading dislocations by epitaxial lateral overgrowth (ELO), a uniform diamond seed layer was formed by bias-enhanced nucleation and then patterned using a dot-shaped Al mask combined with Ar plasma etching. After 100 h of growth and polishing, a diamond film approximately 330 µm thick was obtained, with a dislocation density of 5.25×10^7 cm^{-2} estimated by etch-pit counting. An MSM photodetector with Ti/Pt interdigitated electrodes was fabricated on the diamond film. The device exhibited an extremely low dark current (8.6×10^{-14} A at 20 V), an ultraviolet/visible rejection ratio of approximately 10^3, a responsivity of 0.34 A W^{-1} at 220 nm, and a detectivity of 5.4×10^{12} Jones. The rise and fall time constants under periodic 220 nm illumination were 0.91 s and 0.43 s, respectively (Fig. 13). These findings confirm the potential of heteroepitaxial diamond as a promising wafer-level solar-blind ultraviolet (SBUV) detection platform.

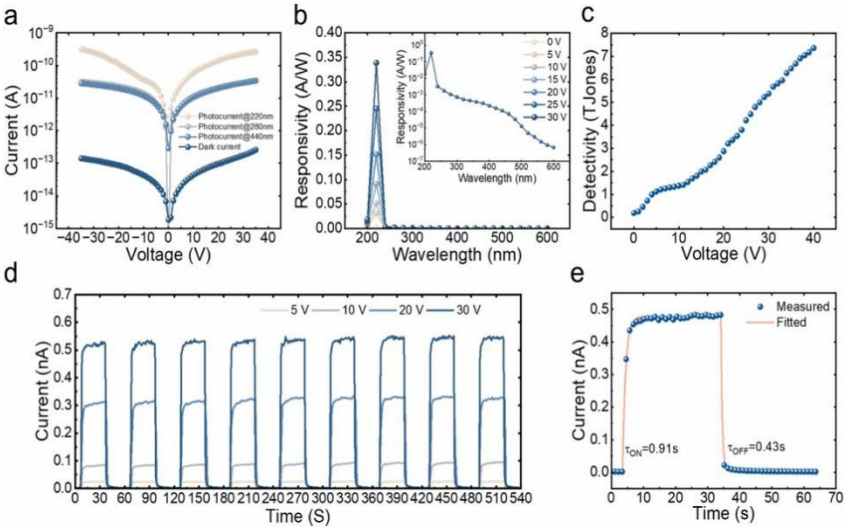


Fig. 13. (a) Dark current and photocurrent under illumination at different wavelengths (illumination area: 4 × 10 mm^2, the device shows the strongest photoexcitation at 220 nm), (b) photoresponsivity under different bias voltages at room temperature (the UV/vis rejection ratio at 20 V is approximately 10^3), (c) detectivity under 220 nm illumination, which increases with bias voltage, (d) switching behavior under different voltages with a period of 1 min (30 s on + 30 s off) at 220 nm (higher voltage improves the switching ratio), (e) fitting of the rise and decay constants at 30 V in (d): 0.91 s and 0.43 s, respectively. Reprinted with permission from Ref. [38].

6. Challenges in Stress and Defect Control of Single-Crystal Diamond Epitaxy on Sapphire Substrates

In recent years, many breakthroughs have been achieved in inch-level (111)-plane single-crystal diamond. However, from the viewpoint of industrial electronic device applications, high stress and high defect density remain major challenges. First, the large thermal expansion mismatch between diamond and sapphire induces very high stress in the film, and the need for stress control becomes more urgent as the wafer size increases. In conventional CVD processes, the substrate temperature typically ranges from 800 to 950 °C, which makes this problem particularly severe [14]. For deposition at 900 °C, the diamond film on sapphire has a compressive strain of approximately 0.45%, and the induced stress is approximately 5 GPa. Owing to the characteristics of MPCVD equipment, transverse and longitudinal temperature gradients exist during epitaxial growth. On one hand, the plasma has an ellipsoidal shape and tends to concentrate at the substrate edge, resulting in a non-uniform temperature distribution across the substrate surface. On the other hand, the substrate's upper surface is in direct contact with the plasma while its lower surface contacts the cooling stage, creating a longitudinal temperature gradient during high-temperature growth. In addition, the lack of chemical affinity between the film and the substrate prevents the formation of an interfacial carbide “glue” layer, resulting in poor adhesion. This readily leads to delamination of the weakly bonded diamond film on the sapphire substrate. Second, CVD diamond growth proceeds under non-thermodynamic-equilibrium conditions, and defects can be generated during deposition. One type is non-epitaxial growth defects: because the edges of the single-crystal diamond substrate attract the plasma, the electric field tends

to concentrate there, causing locally elevated temperatures and, consequently, polycrystalline growth at the edges. Another type is epitaxial growth defects, also known as lattice defects. The lattice mismatch between the heteroepitaxial substrate and diamond introduces a large number of defects, such as dislocations and twins [39]. Meanwhile, impurity elements in the growth chamber (nitrogen, boron, hydrogen, etc.) substitute for carbon atoms, and the resulting vacancies or interstitials lead to high concentrations of point defects.

Dong et al. found obvious local peeling and bulging of the iridium surface after bias-enhanced nucleation on Ir/MgO substrates for heteroepitaxial diamond growth (Fig. 14a) [13]. Furthermore, the large orientation difference between nuclei in the bulging regions made grain coalescence difficult after 20 h of growth, forming grain boundaries and cracks (Fig. 14b). Reciprocal space XRD measurements showed that the Ir film had in-plane compressive strain and out-of-plane tensile strain (Fig. 14c). First, during cooling from the BEN temperature to room temperature, MgO undergoes more pronounced thermal shrinkage, inducing in-plane compressive strain in the Ir film. Second, plasma bombardment creates a steep thermal gradient between the iridium surface and the water-cooled substrate stage. When the accumulated thermal stress exceeds the interfacial bonding energy, delamination is induced (Fig. 14d). High-temperature post-annealing of the sputtered Ir film at 1100 °C effectively suppressed delamination after the BEN process (Fig. 14e), which was attributed to improved film crystallinity and the release of internal stress through Ir migration at high temperature (Fig. 14f). On this basis, a free-standing single-crystal diamond of 10 × 10 mm^2 was obtained (Fig. 14g), with size and crystalline quality roughly equivalent to those of diamond grown on MgO substrates reported in the literature (Fig. 14h).

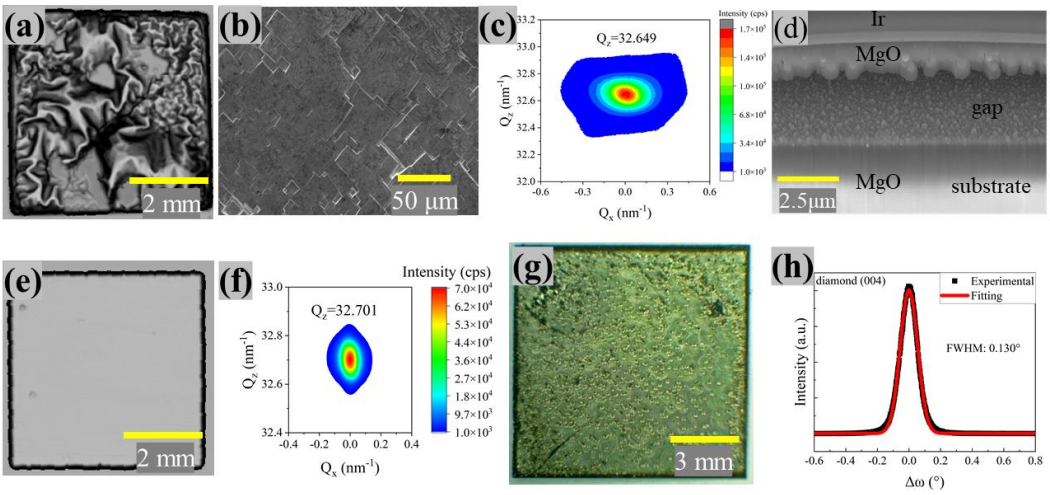


Fig. 14. Surface morphology of Ir/MgO substrates after bias-enhanced nucleation (a) and after growth (b), transverse and longitudinal thermal stress (c) leading to bulging and delamination of MgO (d), high-temperature post-annealing in a tube furnace effectively improves the interface state (e) and suppresses stress (f), the obtained single-crystal diamond is crack-free (g) and exhibits good crystalline quality (h). Reprinted with permission from Ref. [13].

Patterned-mask-assisted lateral epitaxial growth is a common technique for controlling stress and defects in epitaxial materials and has been widely used in other semiconductors and in (100) single-crystal diamond growth. In 2026, Nam et al. alleviated the residual stress in heteroepitaxial diamond growth and improved the crystal quality by introducing a SiO_2 nanosphere (SNS) interlayer [40]. An Ir(100) layer was sputter-deposited on a commercial A-plane sapphire substrate (15 × 15 × 0.67 mm^3, 7° off-axis along the c-direction), and a DC plasma was then used to form uniformly oriented diamond nuclei. A dispersion of 500-nm SiO_2 nanospheres in dimethylformamide was spin-coated onto the substrate (Fig. 15a and 15b), followed by diamond regrowth in an MPCVD system for 70 h. The average vertical growth rate was approximately 7-8 μm/h in both cases, indicating that the SNS interlayer did not adversely affect the growth efficiency. To clarify the role of the SNS as a growth mask, an initial growth experiment of 3 min was carried out. As shown in Fig. 15c, diamond growth was selectively initiated in the gaps between the nanospheres, while growth on the SNS surface was inhibited. The SNS was successfully embedded at the diamond/substrate interface and was not etched by hydrogen plasma (Fig. 15d). The curvature radius of the SNS-assisted film (229.4 cm), calculated with the modified Stoney formula, was almost twice that of the conventional film (127.2 cm), clearly indicating a significant reduction in macroscopic stress. From the Raman shift, a small compressive stress of 0.15 GPa was calculated for the with-SNS (W/SNS) sample. In contrast, the without-SNS (W/O SNS) sample showed a significant blue shift, corresponding to a residual stress of 0.67 GPa. These results clearly indicate that the SNS interlayer effectively alleviates thermal mismatch stress and ensures high spatial uniformity during wafer scaling.

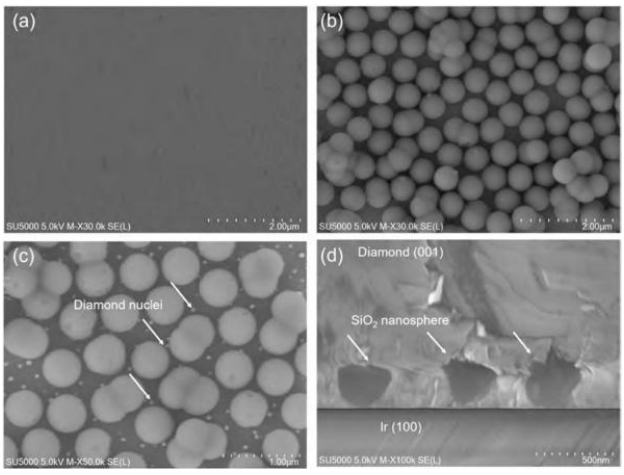


Fig. 15. SEM image of the BEN surface on the Ir/sapphire template (a), SiO_2 nanospheres on the BEN-treated surface (b), initial stages of diamond growth (c), and diamond/SNS/substrate interface (d). Reprinted with permission from Ref. [40].

7. Conclusion and Outlook

Diamond is regarded as the ultimate semiconductor material owing to its exceptional properties, including an

ultra-wide bandgap, high breakdown electric field, and superior thermal conductivity. Heteroepitaxial growth of single-crystal diamond on sapphire substrates has attracted considerable attention due to its scalability to large diameters, with sapphire-based heteroepitaxial wafers currently reaching up to 2 inches. The Ir/sapphire system has emerged as the dominant choice, benefiting from favorable lattice matching, thermal stability, and resistance to carbide formation. By adjusting the miscut angle of the sapphire substrate, annealing conditions, and Ir deposition temperature, Ir thin films with either (001) or (111) orientation can be achieved. For (001)-oriented diamond, techniques such as microneedle seeding, Pd buffer layers, and step-flow growth have enabled the fabrication of free-standing single crystals up to 1-2 inches in size, with dislocation densities reduced to the order of 10^7 cm^{-2}. For (111)-oriented diamond, twin-free films with a lateral size of 30 × 30 mm^2 have been obtained using miscut sapphire substrates (off-cut along the a-axis) to suppress twinning, with a rocking-curve FWHM as low as 94 arcsec. Looking toward industrial-scale adoption, although strategies such as SiO_2 nanosphere interlayers, post-growth high-temperature annealing, and patterned masking can significantly reduce stress and dislocation density, stress and defect control in diamond wafers of 4 inches and beyond remains a major challenge. As heteroepitaxial technologies continue to advance, single-crystal diamond materials are expected to unleash broad application potential in power electronic devices, quantum sensing, and deep-ultraviolet optoelectronic devices.

Author Contributions: We declare that all authors made substantial contributions to this study. Genzhuang Li and Liuan Li jointly proposed the concept of this review. Genzhuang Li designed a systematic literature search protocol and drafted the initial manuscript. Xuejun Li and Tiannan Chen were responsible for literature screening and figure preparation. Weiwei Hu provided critical revisions to enhance the overall depth and logical structure of the paper. Aochen Du, Lai Wei, and Liuan Li (corresponding authors) oversaw the entire project, guided the research process, and reviewed the final draft. All authors participated in discussions and revisions of the manuscript, and approved its submission.

Declaration of competing interest: The authors declare that they have no known competing financial interests or personal relationships that could have appeared to influence the work reported in this paper.

Data Availability Statement: Not applicable.

Funding: This research was funded by Research Start-up Funding of the Organization and Personnel Department, Yili Normal University (No. 2024RCYJ36) and the Key Research and Development Program Special Project of Xinjiang (No. 2024B04033).

Declarations: Ethics, Consent to Participate, and Consent to Publish declarations: not applicable.

References

1. Li, G. Z.; Lin, W.; Liu, S. S.; Aileplanm, Y.; Du, A. C.; Li, L. A., Recent Developments and Challenges of Edge Termination Techniques for Vertical Diamond Schottky Barrier Diodes. *Sensors* **2025,** *25* (22), 6974.

2. Saito, W., A Future Outlook of Power Devices From the Viewpoint of Power Electronics Trends. *IEEE Transactions on Electron Devices* **2024,** *71* (3), 1356-1364.

3. Shikata, S., Single crystal diamond wafers for high power electronics. *Diamond & Related Materials* **2016,** *65* (5), 168-175.

4. CaoYuan., M.; Yi., L. X.; Liang., W. Q.; Xue., L.; Hua., F.; Yu., C. J.; An., L. L.; Zou, B.; Tian., Z. G., Mosaic growth and characteristics of 2-inch single-crystal diamond. *Functional Diamond* **2026,** *6* (1), 2620820.

5. Li, G. Z.; Li, D. S.; Mu, C. Y.; Wang, Q. L.; Lv, X. Y.; Li, L. A.; Zou, G. T., Effect of step-flow modulation on the large-size single crystal diamond through mosaic growth. *Functional Diamond* **2023,** *3* (1), 2279057.

6. Matthias Schreck, S. G., Rosaria Brescia, Martin Fischer Ion bombardment induced buried lateral growth: the key mechanism for the synthesis of single crystal diamond wafers. *Scientific Reports* **2017,** *7* (1), 44462.

7. Gsell., S.; Bauer., T.; Goldfug., J.; Schreck., M.; Stritzker., B., A route to diamond wafers by epitaxial deposition on silicon via iridium/yttria-stabilized zirconia buffer layers. *Applied Physics Letters* **2004,** *84* (22), 4541-4543.

8. Bauer., T.; Gsell., S.; Schreck., M.; Goldfug., J.; Lettieri., J.; Schlom., D. G.; Stritzker., B., Growth of epitaxial diamond on silicon via iridium/$SrTiO_3$ buffer layers. *Diamond & Related Materials* **2005,** *14* (3-7), 317-317.

9. Tachibana., T.; Yokota., Y.; Kobashi., K.; Yoshimoto., M., Heteroepitaxial growth of {111}-oriented diamond fims on platinum {111}/sapphire {0001} substrates. *Journal of Crystal Growth* **1999,** *205* (1-2), 163-168.

10. Tachibana., T.; Yokota., Y.; Kobashi., K.; Hayashi., K., Growth of {111} -oriented diamond on Pt/Ir/Pt substrate deposited on sapphire. *Diamond & Related Materials* **2001,** *10* (9-10), 1633-1636.

11. Wei., L.; Tucker., D. A.; Chun., Y. P.; Glass, J. T., Nucleation of oriented diamond particles on cobalt substrates. *Journal of Applied Physics* **1995,** *77* (2), 1291-1296.

12. Ohtsuka., K.; Suzuki., K.; Sawabe., A.; Inuzuka., T., Epitaxial Growth of Diamond on Iridium. *Japanese Journal of Applied Physics* **1996,** *35* (8B), 1072-1074.

13. Dong, C. W.; Zhang, K.; He, L.; Liu, J. W.; Zhang, Z. H.; Lv, X. Y.; Wang, Q. L.; Li, L. A.; Zou, G. T., Interfacial improvement of Ir/MgO substrate by post-deposition annealing for heteroepitaxial growth of single crystal diamond. *Journal of Alloys and Compounds* **2025,** *1036* (7), 182174.

14. Singha., R. K.; Gilbert., D. R., Growth of adherent diamond films on optically transparent sapphire substrates. *Applied Physics Letters* **1996,** *69* (15), 2181-2183.

15. Saw., K. G.; Andrienko., I.; Cimmino., A.; Spizzirri., P.; Prawe., S.; Plessis., J. D., Growth of diamond on α-(0001) sapphire substrates. *Diamond & Related Materials* **2003,** *12* (10-11), 1663-1669.

16. Roberto., V.; Takashi., G.; Wei., Z.; Toshio., H., Epitaxial growth of iridium and platinum films on sapphire by metalorganic chemical vapor deposition. *Applied Physics Letters* **1994,** *65* (9), 1094-1096.

17. Bednarski-Meinke., C.; Dai., Z.; Li., A. P.; Golding., B., Studies of heteroepitaxial growth of diamond. *Diamond & Related Materials* **2003,** *12* (3-7), 241-245.

18. Dai., Z.; Bednarski-Meinke., C.; Loloee., R.; Golding., B., Epitaxial (100) iridium on A-plane sapphire: A system for wafer-scale diamond heteroepitaxy. *applied Physics Letters* **2003,** *82* (22), 3847-3849.

19. Dai., Z.; Bednarski-Meinke., C.; Golding., B., Heteroepitaxial diamond film growth: the a-plane sapphire–iridium system. *Diamond & Related Materials* **2004,** *13* (4-8), 552-556.

20. Samoto., A.; Ito., S.; Hott., A.; Hasebe., T.; Ando., Y.; Sawab., A.; Suzuki., T., Investigation of heterostructure between diamond and iridium on sapphire. *Diamond & Related Materials* **2008,** *17* (7-10), 1039-1044.

21. Frank., M.; Sabine., O.; Andreas., G.; Eduard., R.; Eva-Regine., C.; Alexander., F.; Marco., W.; Lukas., G.; Frank., B., Effect of substrate bias on the growth behavior of iridium on A-plane sapphire using radio frequency sputtering at low temperatures. *Thin Solid Films* **2018,** *650* (6), 65-70.

22. Hua., W. W.; Lin., Y. S.; Cai., H. J.; Bing., D.; Qi., Z. J., Role of surface chemistry in determining the heteroepitaxial growth of Ir films on a-plane α-Al_2O_3 single crystals. *Surfaces and Interfaces* **2022,** *32* (5), 102172.

23. Vedaste., U.; Liu., C.; Qian., S. Z.; Yu., X. X.; Lang., W. H.; Xing., Z.; H.L.., Z. K., Growth of high-quality Ir thin films with controlled crystal orientations on α-plane sapphire substrates. *Applied Surface Science* **2026,** *737* (23), 166872.

24. Seong-Woo., K.; Yuki., K.; Ryota., T.; Koji., K.; Kasu, M., Growth of high-quality one-inch freestanding heteroepitaxial (001) diamond on (11 0) sapphire substrate. *Applied Physics Letters* **2020,** *117* (20), 202102.

25. Hideo., A.; Seong-Woo., K.; IkejiriKenjiro.; Yuki., K.; Koji., K.; Hideyuki., K.; Atsuhito., S., Fabrication of freestanding heteroepitaxial diamond substrate via micropatterns and microneedles. *Applied Physics Express* **2016,** *9* (3), 035504.

26. Wei, Q.; Lin, F.; Wang, R. Z.; Zhang, X. F.; Chen, G. Q.; Hussain, J.; He, D.; Zhang, Z. Y.; Niu, G.; Wang, H. X., Heteroepitaxy growth of single crystal diamond on Ir/Pd/Al_2O_3 (11-20) substrate. *Materials Letters* **2021,** *303* (22), 130483.

27. Seong-Woo., K.; Ryota., T.; Shintaro., H.; Makoto., K., Two-inch high-quality (001) diamond heteroepitaxial growth on sapphire (11-20) misoriented substrate by step-flow mode. *Applied Physics Express* **2021,** *14* (11), 115501.

28. Yonhua., T.; Jian-Wei., T.; Lun., C. I.; Che., H. C., DC bias enhanced heteroepitaxial nucleation of (100) diamond on Ir(100)/ a-sapphire by 915 MHz microwave plasma chemical vapor deposition. *Thin Solid Films* **2026,** *833* (1), 140839.

29. Yonhua., T.; Cheng., C. J.; Lun., C. I.; Han., W. B.; Lung-Hsin., H.; Pao., C. C.; Che., H. C., RF bias-enhanced heteroepitaxial nucleation of (100) diamond on (100) Ir/a-sapphire. *Journal of Applied Physics* **2026,** *139* (9), 095301.

30. Shimaoka, T.; Yamada, H.; Chayahara, A., Fabrication of self-standing large (111) single crystal diamond using bulk growth of (100) CVD diamond and lift-off process. *Diamond & Related Materials* **2024,** *142* (2), 110781.

31. Xi., F. W.; Ting., W. K.; Aoi., M.; Xing., W. H.; Hiroshi., K., Local initial heteroepitaxial growth of diamond (111) on Ru (0001)/c-sapphire by antenna-edge-type microwave plasma chemical vapor deposition. *Applied Physics Letters* **2020,** *117* (11), 112102.

32. Choi, U.; Shin, H.; Kwak, T.; Kim, S.-W.; Nam, O., Growth and characterization of heteroepitaxial (001) and (111) diamond on Ir/sapphire structures. *Diamond & Related Materials* **2022,** *121* (1), 108770.

33. Taemyung., K.; Seolyoung., O.; Yoonseok., N.; Hyeonu., K.; Geunho., Y.; Okhyun., N., Twin-free (111) single-crystal diamond heteroepitaxially grown on (1-102) sapphire substrate. *Diamond & Related Materials* **2025,** *159* (9-10), 112857.

34. Seong-Woo., K.; Yuki., K.; Kohei., H.; Jeffery., A.; Koji., K.; Mariko., S., Freestanding 30 mm square {111} twin-free heteroepitaxial diamonds grown on highlymisoriented {0001} sapphire substrates. *Applied Physics Express* **2026,** *19* (3), 031003.

35. Taemyung., K.; Jonggun., L.; Uiho., C.; Byeongchan., S.; Geunho., Y.; Seongwoo., K.; Okhyun., N., Diamond Schottky barrier diodes fabricated on sapphire-based freestanding heteroepitaxial diamond substrate. *Diamond & Related Materials* **2021,** *114* (4), 108335.

36. Chen, G. q.; Wang, W.; Lin, F.; Zhang, M. H.; Wei, Q.; Yu, C.; Wang, H. X., Electrical Characteristics of Diamond MOSFET with 2DHG on a Heteroepitaxial Diamond Substrate. *Materials (Basel)* **2022,** *15* (7), 2557.

37. Chandra., S. N.; Seong-Woo., K.; Koji., K.; Toshiyuki., O.; Makoto., K., 3659-V NO_2 p-Type Doped Diamond MOSFETs on Misoriented Heteroepitaxial Diamond Substrates. *IEEE Electron Device Letters* **2023,** *44* (1), 112-115.

38. Zhu, H.; Yang, S. L.; Cheng, C. F.; Fan, S. F.; Zheng, Y. T.; Dai, B.; Li, Y. C.; Zhu, J. Q., Mechanism analysis of large-scale heteroepitaxial diamond solar-blind ultraviolet photodetectors with ultralow dark current. *Carbon* **2026,** *248* (3), 121082.

39. Bensalah., H.; Stenger., I.; Sakr., G.; Barjon., J.; Bachelet., R.; Tallaire., A.; Achard., J.; Vaissiere., N.; Lee., K. H.; Saada., S.; Arnault, J. C., Mosaicity, dislocations and strain in heteroepitaxial diamond grown on iridium. *Diamond & Related Materials* **2016,** *66* (6), 188-195.

40. Yoon., M.; Kwak., T.; Jeong., J.; Oh., S.; Nam., Y.; Yoo., G.; Nam., O., Heteroepitaxial growth of (100) single-crystal diamond with reduced wafer bow via SiO_2 Nanospheres interlay. *Diamond & Related Materials* **2026,** *164* (4), 113468.